LAWRENCE
LIVERMORE
NATIONAL
LABORATORY

Fabrication and testing of germanium grisms for LMIRcam

P. J. Kuzmenko, S. L. Little, L. M. Little, J. C. Wilson, M. F. Skrutskie, P. M. Hinz, J. M. Leisenring, O. Durney

July 2, 2012

Disclaimer

This document was prepared as an account of work sponsored by an agency of the United States government. Neither the United States government nor Lawrence Livermore National Security, LLC, nor any of their employees makes any warranty, expressed or implied, or assumes any legal liability or responsibility for the accuracy, completeness, or usefulness of any information, apparatus, product, or process disclosed, or represents that its use would not infringe privately owned rights. Reference herein to any specific commercial product, process, or service by trade name, trademark, manufacturer, or otherwise does not necessarily constitute or imply its endorsement, recommendation, or favoring by the United States government or Lawrence Livermore National Security, LLC. The views and opinions of authors expressed herein do not necessarily state or reflect those of the United States government or Lawrence Livermore National Security, LLC, and shall not be used for advertising or product endorsement purposes.

Fabrication and testing of germanium grisms for LMIRcam

Paul J. Kuzmenko[*a], Steve L. Little[a], Liesl M. Little[a], John C. Wilson[b], Michael F. Skrutskie[b], Phillip M. Hinz[c], Jarron M. Leisenring[d], and Oliver Durney[c]

[a]Lawrence Livermore National Laboratory, L-183 PO Box 808, Livermore, CA 94551;
[b]University of Virginia, 530 McCormick Rd., Charlottesville, VA 22904;
[c]University of Arizona/Steward Observatory, 933 N. Cherry Ave., Tucson, AZ 85721;
[d]ETH Zurich, Building HIT, Floor J, Wolfgang-Pauli-Strasse 27, 8093 Zurich, Switzerland

ABSTRACT

We diamond fly cut 2 sets of germanium grisms for the LMIRcam 3-5 micron Fizeau imager for the combined focus of the Large Binocular Telescope (LBT). The grisms mount in a filter wheel near a pupil to enable moderate resolution (R~300) spectroscopy. Both sets have a measured blaze angle of 2.9º. The first set has a groove period of 40 lines/mm and will be used in first order with peak efficiency at 3.6 μm. The second set has 32 lines/mm. It can operate in first order with an efficiency peak near 4.4 μm and in second order with a peak near 2.3 μm. First results from testing the grisms in the instrument on the sky with the LBT are presented.

Keywords: infrared, grism, germanium, LMIRcam

1. INTRODUCTION

The L/M-band Infrared Camera (LMIRcam) is a 3-5 micron Fizeau imager for the combined focus of the Large Binocular Telescope (LBT). LMIRcam[1,2] reimages the interferometrically combined coherent focus of the LBT using an extensive set of broad and narrow-band filters throughout the mid-infrared. The imager resides within the University of Arizona's Nulling Infrared Camera (NIC) and follows the University of Arizona's Large Binocular Telescope Interferometer (LBTI) which sits between the primary mirrors on the binocular mount and interferometrically combines the light collected from each aperture after only three warm mirror reflections per side (primary, adaptive secondary, and tertiary). LMIRcam, developed by the University of Virginia, the University of Arizona, the University of Minnesota and Notre Dame, is being commissioned at the LBT after achieving first light in May 2011.

The central fringe and first interferometric null at 3.6 micron wavelength from the combined light of the LBT's 8.4-m primary mirrors (with 14.4-m separation) are separated by 26 milliarcseconds on the sky. Such high spatial resolution, along with the low thermal background that comes with the use of only a few warm mirrors, should allow a variety of science uses including the detection of warm "Jupiters" in nearby young systems, the study of star formation and debris disks, and the study of ultra-luminous infrared galaxies.

Along with its suite of filters, LMIRcam includes two diamond machined germanium grisms to allow moderate resolution (R~300) spectroscopy in the mid-infrared. The grisms were recently fabricated and installed in the instrument for first tests on the sky prior to anti-reflection (AR) coating and are the subject of this paper. Grism design and design verification through electromagnetic modeling are covered in section 2. Section 3 describes the steps used in fabricating the grisms. In section 4 tests on the uncoated grisms are described and discussed. Conclusions and tasks for future work are presented in section 5.

2. DESIGN AND MODELING OF THE GRISMS

The grism parameters are determined by the optical design, which in turn is driven by scientific requirements. Moderate resolution (R~ 300) provides the greatest scientific utility. We need grisms operating in first order to achieve peak efficiency at the centers of the L and M photometric bands. This means that two different grisms are required. To permit

[*]kuzmenko1@llnl.gov; phone 925-423-4346; fax 925-422-2499

use at shorter wavelengths we adjusted the blaze wavelength for M-band grism so that in second order the peak efficiency is in a desirable location on the long wavelength side of K-band. We chose designs in which the prism apex angle equals the blaze angle so that the central wavelength is undeviated in transmission. Fixed parameters include pupil diameter (6.4 mm) and the individual telescope diameter aperture (8.4 m). We selected a slit size projected on the sky of 0.033 arcsec to take advantage of the excellent spatial resolution expected from interferometric combination. Lastly, for manufacturing simplicity we went with a common prism/blaze angle.

The original design used KRS-5 as the grism material. At LLNL we had no experience working with KRS-5 and its toxicity would have been problematic. So we chose single crystal germanium, which is easily diamond machined and which we had used in a number of immersion gratings[3,4]. It offers a high index, good thermal properties, and is readily available.

The gratings were designed using classic grism equations to optimize for performance on three bands. The grism parameters (namely groove density and prism angle) were derived using equations in section 2 of Jeremy Allington-Smith's tutorial[5]. Rayner determines parameters in a similar way and his paper is also a good reference[6].

The grism equation states: $$\lambda = ((n-1)*\sin(\alpha))/(m\rho), \tag{1}$$

where λ is the blaze wavelength in air, n is the refractive index of the grism material, α is the angle of incidence on the grating surface and the prism apex angle, m is the diffraction order and ρ is the groove density (inverse of the groove spacing).

The equation for spectral resolution R is:

$$R = (m*\lambda*D_{pupil}*\rho)/((\cos(\alpha)*\phi_{slit}*D_{telescope}), \tag{2}$$

Where D_{pupil} is the pupil diameter, $D_{telescope}$ is the diameter of the telescope aperture and ϕ_{slit} is the angular size of the slit projected on the sky. These can be combined to yield an expression for the prism angle:

$$\alpha = \arctan((R*\phi_{slit}*D_{telescope})/(D_{pupil}*(n-1)). \tag{3}$$

These equations were entered into an Excel spreadsheet and the parameters were iteratively adjusted until all the constraints and equations were consistent. Final design parameters are presented in Table 1.

Table1. LMIRcam grism specifications derived from classic grism equations

Grism 1	Grism 2
L band (peak at 3.6 μm), 1st order	M band (peak at 4.4 μm), 1st order
	K band (peak at 2.3 μm), 2nd order
40.0 grooves/mm	32.0 grooves/mm
2.8° blaze angle	2.8° blaze angle

To verify that optics fabricated with the designed blaze and prism angles would perform as expected and to calculate transmission efficiencies, the grisms were modeled using GSolver©, a commercial diffraction grating analysis program. GSolver does not model bulk optics, so the model begins within the germanium prism. Reflective losses at the entrance face of the prism are not modeled, so the transmission efficiency calculations include only the grating surface. The angle of incidence at the grating surface equals the prism apex angle.

GSolver offers three built-in refractive index models for Ge. However, these built-in models do not cover the wavelength range of interest. The models for these grisms were based on a user-supplied table-style model for the Ge refractive index at 80K, covering the range 1.92 to 5.98 µm and extrapolated from published data[7].

The grism modeling assumes a 90º angle between the groove facets with a perfectly sharp, zero radius corner. This is not unreasonable as radii of less than 0.1 µm have been achieved with a dead sharp tool[4]. The results of the model calculations for both incident polarizations are shown in figure 1. Each band peaks at or very close to the design wavelength. The maximum diffraction efficiencies are roughly 0.62, which is close to the transmission of a germanium-air interface. So the efficiencies are limited by reflective losses due to the high refractive index of germanium, and not by the design of the grism, or deficiencies in the groove shape. Near the peak of the efficiency curve the fraction of incident light coupled into other diffractive orders is small.

Thus the efficiencies have the potential for significant increase using antireflection coatings. GSolver has the ability to model these coatings, but the specific composition and thickness of the layers in an antireflection coating varies to some extent between coating vendors. Since a specific vendor had not been identified at the time the models were completed, the effects of the coatings were not included.

A final step before fabrication is the specification of tolerances for the grism design. Modeling shows that the predicted efficiency curve is only weakly affected by a ± 0.25º change in the prism apex angle. It is more sensitive to changes in the blaze angle. A ± 0.25º variation in blaze angle shifts the efficiency peak by 0.2 to 0.4 µm depending on the grism and order of operation. So we set the blaze angle tolerance at ± 0.1º.

3. FABRICATION

LLNL has diamond-machined a number of gratings in germanium for internal projects. These have blaze angles of the order a few degrees and clear apertures of approximately 1 cm^2. Two earlier publications describe the fabrication details[3,4]. The LMIRcam grisms have roughly twice the area of our previous gratings.

Germanium has low absorption in the 2 to 5 µm range. This allows the grism blanks to be sufficiently thick to resist deformation while being mounted into the machining fixture. Six single crystal germanium blanks, 5 mm thick and 16 mm square with a 2.8º wedge angle, were obtained from Umicore Optical Materials. The crystal orientation is specified to produce optimal cutting conditions. See reference 3 for the full details. The blanks were delivered with rough ground surfaces and Nu-Tek Precision Optical Corporation polished the flat entrance faces.

Once the germanium blanks are received and inspected, a polishing etch is used to remove about 50 µm of material. This eliminates layers with subsurface damage from the cutting and grinding of the blanks and produces a defect free surface ready for machining. The polished entrance face is protected with optical wax (30% beeswax and 70% rosin) during the etching (see figures 2, 3 and 4). Figures 5 and 6 show a blank after etching. Some of the periphery of the polished entrance face was etched where the wax pulled back from the edge, but these regions are outside the clear aperture.

Proper fixturing of the germanium blank is essential to achieving the lowest wavefront error in the grating surface. It must be held rigidly but stress free so that there will be no spring back deformation when removed from the machining fixture. We use a steel fixture with the prism apex angle machined into the top surface. This allows the grooves to be cut into a horizontal plane at the proper angle with respect to the entrance face. Support for the blank is provided by three 1 mm^2 pads machined into the inclined surface. Cyanoacrylate adhesive fastens the blank to the pads. There are 3 steel dowel pins pressed into the inclined surface to fix the horizontal position and rotation of the germanium with respect to the reference surfaces of the machining fixture.

There is significant CTE (coefficient of thermal expansion) mismatch between the germanium blank and its carbon steel machining fixture. It is very important to eliminate any differences in temperature between the blank and its fixture while it is being glued in place. It is also important to minimize any change in temperature of the fixture from the time when the blank is glued in place until it is installed in the machine and cutting commences.

Several steps are taken to mitigate this problem. The PERL (Precision Engineering Research Lathe), a diamond turning machine used to cut the gratings, resides in an enclosure which is temperature controlled to 0.01ºC. This enclosure sits in a room which is temperature controlled to about 0.2ºC. The germanium blank is placed on the support pads of the steel fixture and both are placed in the PERL enclosure overnight. This allows blank and fixture to come to thermal equilibrium with each other and with the machine.

It is very important to prevent the body heat of the machinist from perturbing this thermal equilibrium while fastening the blank into the machining fixture. We have developed a handling fixture consisting of a small metal block in which are installed 3 tapered metal pins. The thermal mass of the metal block, the low thermal conductivity of the tapered pins, and the small contact area with the grating blank greatly diminish the heat flow into the blank.

To use the handling fixture a small amount of cryanoacrylate adhesive is applied to the tips of each of the 3 pins. With the germanium blank resting on the three mounting pads of the machining fixture and properly located by the dowel pins the handling fixture is slowly lowered onto the upper surface of the blank. Care is taken to position the pins of the handling fixture directly above the mounting pads of the machining fixture so that no bending moment is applied to the grating blank. The cyanoacrylate adhesive bonds in few seconds and gains full strength over several minutes. At this point the blank is lifted off the machining fixture (see figure 7). All parts are allowed to return to thermal equilibrium with PERL.

To complete the fixturing process, cyanoacrylate adhesive is applied to each of the 3 mounting pads on the machining fixture. The handling fixture is used to slowly lower the germanium blank onto the mounting pads, keeping the pins well aligned with the pads (see figure 8). Although cyanoacrylate adhesive reaches full bond strength in a few minutes it does not achieve full chemical resistance for 24 hours so the assembly is left inside the PERL enclosure overnight. The handling fixture is unglued before machining with a chemical release agent.

Next the machining fixture is mounted onto the x-translation stage of PERL (see figure 9). Fine pitch jacking screws in the fixture allow very precise leveling of the top surface (to 1 μm over 1 cm of translation). This means that the apex angle of the grism will be as precise as the angle of inclined surface machined into the fixture. To perform this operation an electronic indicator gauge is magnetically attached to the spindle block and made to contact the top surface of the fixture. As the fixture is translated along the x-direction, changes in surface height indicate an out-of-level condition to be corrected. The reference surface of the fixture is aligned with a similar technique and tolerance to be parallel to the direction of motion of the x-stage.

To machine the grisms a single crystal diamond tipped flycutting tool was purchased from Chardon Tool. The tool specifications called for a dead sharp tip with an included angle of 90º±0.1º, a blaze angle of 2.8º±0.1º, and 30º of negative top rake. We set the tool to cut about 50 μm into the germanium. The grisms are machined under a mist of light mineral oil at 1000 RPM spindle speed and a feed rate of 0.4 inches per minute. After the spindle motor is started, a thermal soak of 12 hours elapses before the PERL axes of motion are engaged. This allows the machine to reach thermal equilibrium before cutting begins. The x-translation stage moves the blank beneath the rotating tool. At the end of travel the spindle position is incremented and the stage moves back, cutting the next groove. Hence the grooves are bidirectionally cut. The machining process takes about 23 hours to complete.

After cutting grism #1 we measured the blaze angle and the apex angle using a HeNe laser and a precision rotation stage with 1 arc minute resolution[8]. The apex angle was 2.8º, which matched the design specifications. But the blaze was 2.3º, which is well out of tolerance. We were able to machine the shank of the cutting tool to compensate for the error. All later grisms measured 2.89º blaze. Grism #1 was recut correctly after etching away the grooves. The source of the error was traced to a miscommunication in the specification of the included angle. Several of the finished grisms may be seen in figure 10. Ultimately six grisms were fabricated – three each with 32 and 40 l/mm groove density, respectively.

4. TESTING OF UNCOATED GRISMS

Upon completion of each of the 6 grisms a number of tests are performed to show that they meet the design specifications and to demonstrate their performance. The first test after the finished grism is cleaned is an optical

inspection under high magnification to look for chipped or pitted grooves. Figure 11, a 500x image of a section of grism #1, shows a typical result.

The next test is a measurement of the blaze angle as described above. While the grooved surface is illuminated with a visible HeNe (i.e. operating the grating in reflection) one can examine the diffraction pattern for ghosts and in-plane scatter. Tests on similarly fabricated gratings at 10.6 μm wavelength[4] failed to reveal ghosts down to an intensity of 0.01%. Since the intensity of Rowland ghosts[9] scale as λ^{-2}, they should be much more noticeable at the shorter wavelengths. At 633 nm we would typically observe one grating ghost halfway between the brightest diffraction order and an adjacent order. This indicates groove position error with a 2 groove periodicity. The ghost intensity varied as the laser moved across the grooved surface but never exceeded 1% of the incident power. We believe that the x-translation stage has a very slight (nanometer level) offset in position depending on its direction of motion. (i.e. left or right) A grating cut unidirectionally on PERL after the completion of these grisms showed no detectable ghosts[10].

A very important measure of grating quality is the surface error. This is the extent to which the diffracted wavefront from an incident plane wave is no longer planar. This aberration limits the size of the focal spot therefore limiting the spectral resolution of the grating. The grisms are tested in reflection (Littrow mode) with a Zygo interferometer, which provides a spatial map of the surface error. The result for grism #6 is shown in figure 12. The surface error at 633 nm over the full 14 x 14 mm aperture was 0.10 λ peak to valley and 0.012 λ rms. The largest surface error for any grism was 0.14 λ peak to valley (0.023 λ rms), which is well within the diffraction limit at 633 nm, let alone the LMIRcam wavelengths.

A final test was to examine the groove surfaces with a scanning electron microscope (SEM). Figures 13 and 14 taken with a Hitachi SU8020 ultrahigh-resolution field emission SEM show very flat smooth groove surfaces as well as a very sharp groove angle.

One of each uncoated grism type was installed in LMIRcam in March 2012 and tested with an internal source and on the sky. Grisms mount in a filter wheel just upstream of the detector at a location adjacent to an image of the instrument Lyot stop. While the grism is used in converging light, it is a slow beam: f/16 envelope for the coherently combined light.

While LMIRcam is currently deployed with slits, initial on-sky tests were conducted in slit-less mode such that the spectral resolution is defined by the FWHM of the AO-corrected PSF's.

Figure 15 shows a preliminary extraction of nod-subtracted fringes of the bright star HD 82198 dispersed by the L-band grism. The observation is a 29 msec integration of the coherently combined light from the AO-corrected telescope apertures. The extraction (median combination of 20 pixels orthogonal to the fringes), shifted and scaled by-eye, compares well to the L-band ATRAN atmospheric transmission model[11] for 1.5 airmasses and 1.0 mm precipitable water (available from the Gemini Observatory website) multiplied by the modeled L-band grism efficiency curve and the transmission curves of a dichroic and order sorting filter in the optical train.

On-sky observations also showed that the dispersed light from the grisms can be used to fine-tune the interferometric phasing between telescope apertures. Figures 16 and 17 give examples of dispersed light both on and off the white-light fringe.

5. CONCLUSIONS AND FUTURE WORK

The uncoated grisms have met their design specifications and have performed well in LMIRcam. However due to Fresnel losses in high index germanium, a large improvement in transmission can be obtained by applying antireflection coatings. Broadband antireflection coatings will be applied to both the entrance face and the machined grating surface of the grisms by Infinite Optics (Santa Ana, CA).

One may question the wisdom of applying an antireflection coating to a grooved surface at the risk of degrading optical performance. Calculations show that one should minimize the coating thickness on the anti-blaze groove facets[12].

Fortunately this is easy to achieve for low blaze angle grisms as the anti-blaze facets are nearly vertical during the coating deposition. Work at UT Austin on the silicon grisms for the JWST NIRCam demonstrates that a broadband (2.0-5.0 µm) antireflection coating can be deposited without significant degradation of performance[13]. Testing of the coated grisms in LMIRcam is planned for later this summer.

ACKNOWLEDGEMENTS

REFERENCES

[1] Leisenring, J.M., Skrutskie, M.F., Nelson, M.J., Wilson, J.C., Hinz, P.M., Hoffman, W.F., Bailey, V., Vaitheeswaran, V., Jones, T.J., Schoenwald, J., and Meyer, M.R., "On-sky operations and performance of LMIRcam at the Large Binocular Telescope," 2012, these proceedings

[2] Skrutskie, M.F., Jones, T., Hinz, P., Garnavich, P., Wilson, J., M. Nelson, Soldheid, E., Durney, O., Hoffmann, W., Vaitheeswaran, V., McMahon, T., Leisenring, J. and Wong, A., "The Large Binocular Telescope mid-infrared camera (LMIRcam): final design and status," Proc. SPIE 7735, 77353H (2010).

[3] Kuzmenko, P. J., Little, L. M., Davis, P. J. and Little S. L., "Modeling, fabrication and testing of a diamond machined germanium immersion grating," Proc. SPIE 4850, 1179-1190 (2002).

[4] Kuzmenko, P. J., Davis, P. J., Little, S. L., Little, L. M. and Bixler, J. V., "High efficiency germanium immersion gratings," Proc. SPIE 6273, 62733T (2006).

[5] Allington-Smith, J., "Dispersive astronomical spectroscopy," available at
www.dur.ac.uk/resources/cfai/jras_papers/spectroscopy-theory.pdf (2002).

[6] Rayner, J. T., "Evaluation of a solid KRS-5 grism for infrared astronomy," Proc. SPIE 3354, 289-294 (1998).

[7] Li, H. H., "Refractive-index of silicon and germanium and its wavelength and temperature derivatives," J. Phys. Chem, Ref. Data 9(3), 561-658 (1980).

[8] Loewen, E. G. and Popov, E., [Diffraction Gratings and Applications], Dekker, New York, 420 (1997).

[9] Palmer, E. W., Hutley, M. C., Franks, A., Verrill, J. F., and Gale, B., "Diffraction Gratings," Reports on Progress in Physics 38, 975-1048 (1975).

[10] Ikeda. Y., Photocoding, Inc., private communication (2011).

[11] Lord, S. D.,, NASA Technical Memorandum 103957 (1992).

[12] Kleemann, B. H. and Erxmeyer, J., "Independent electromagnetic optimization of the two coating thicknesses of a dielectric layer on the facets of an echelle grating in a Littrow mount," Journal of Modern Optics 51, 2093-2110 (2004).

[13] Gully-Santiago, M., Wang, W., Deen, C., Kelly, D., Greene, T. P., Bacon, J. and Jaffe, D. T., "High Performance Silicon Grisms for 1.2-8.0 µm: Detailed Results from the JWST-NIRCam Devices," Proc. SPIE 7739, 77393S (2010).
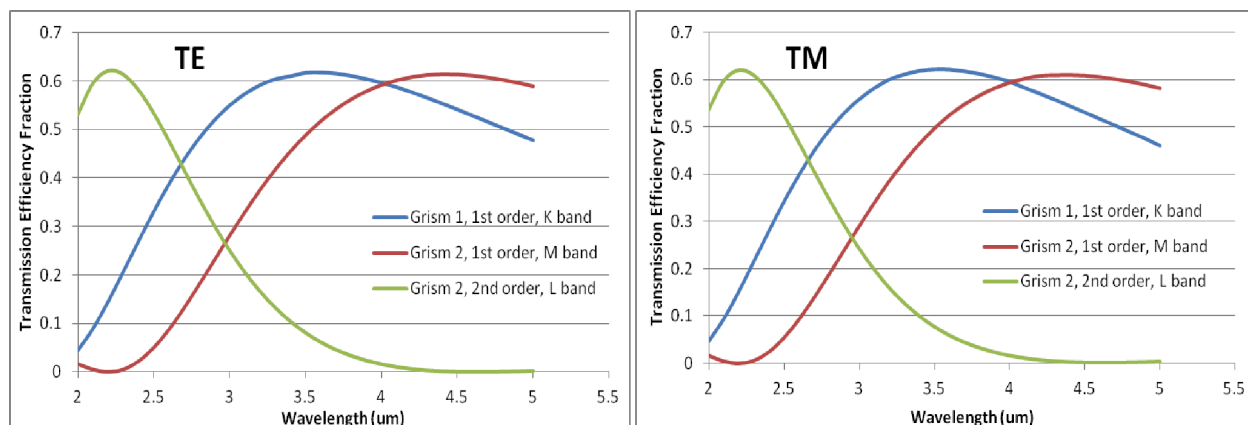
Figure 1. Transmission efficiencies calculated using GSolver for TE and TM incident fields. The calculation assumes that grism 1 has 40 grooves per mm and grism 2 has 32 grooves per mm. Both have a blaze angle of 2.8º. Peak efficiencies are limited by the Fresnel reflectivity of the uncoated groove facets. The entrance face is assumed to have a perfect AR coat.

Figures 2 and 3. Before the grism blanks can be etched to removed the subsurface damage produced during cutting and grinding, the polished entrance face must be masked with a protective wax coating. The left photo shows the blanks being warmed on a hotplate along with a container of molten optical wax (30% beeswax and 70%rosin). The right hand photo shows the blanks slowly cooling after the wax has been applied.
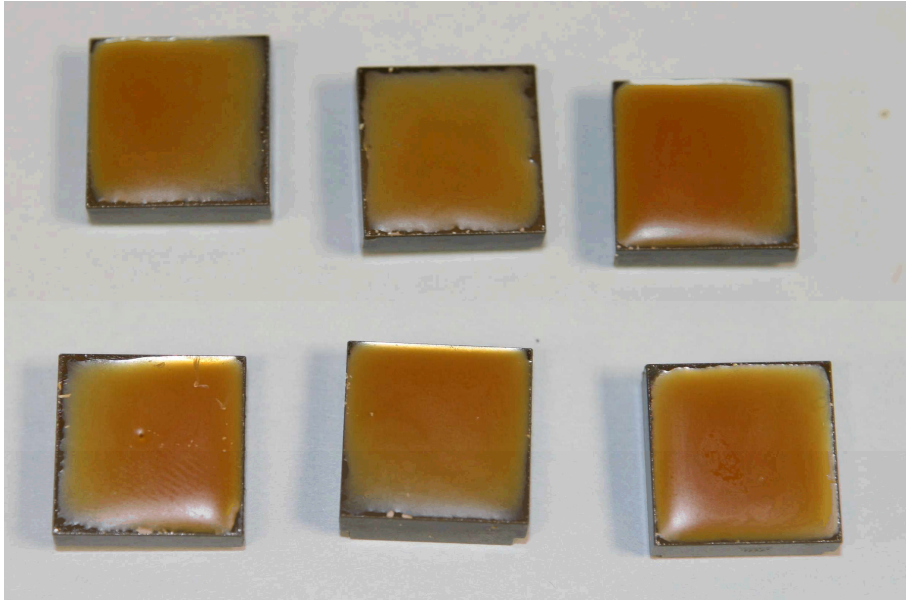
Figure 4. Photograph shows the grism blanks after the wax has solidified. Note that the large contraction during solidification has caused the wax to pull back from the edges of the bank
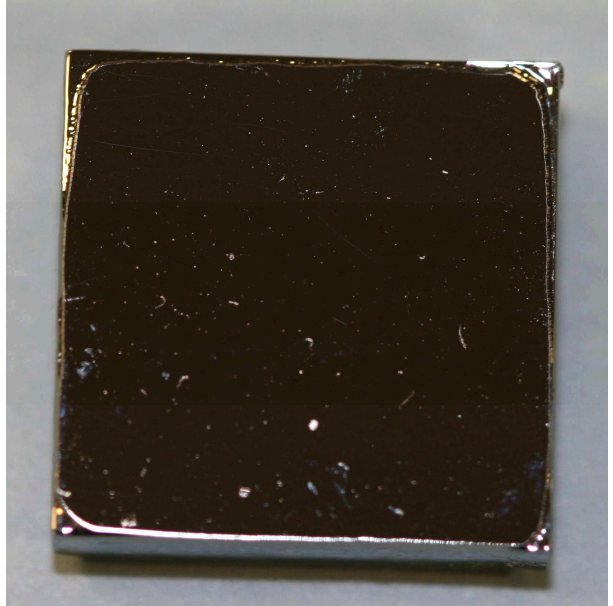
Figures 5 and 6 show a blank after etching. The left photo shows the surface into which a grating will be machined. The original rough ground surface is made shiny by the polishing etch. The right photo shows the polished entrance face after removal of the wax. There is some etching near the periphery.
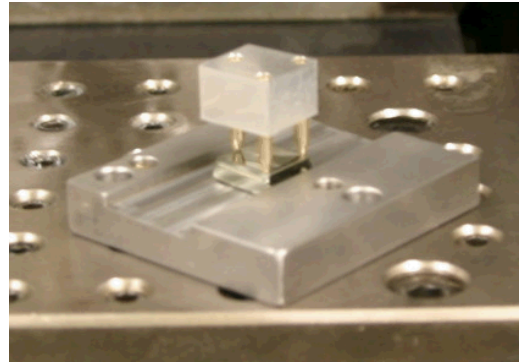
Figures 7 and 8 show the installation of the blank into the machining fixture. At the left, the grating blank is glued to the pins of the handling fixture, which are aligned to be directly above the support pads of the machining fixture. At the right the blank is glued onto the support pads. The handling fixture restricts heat flow into the blank so it remains isothermal with the machining fixture eliminating a source of thermally induced stress. The handling fixture is unglued before machining with a chemical release agent.
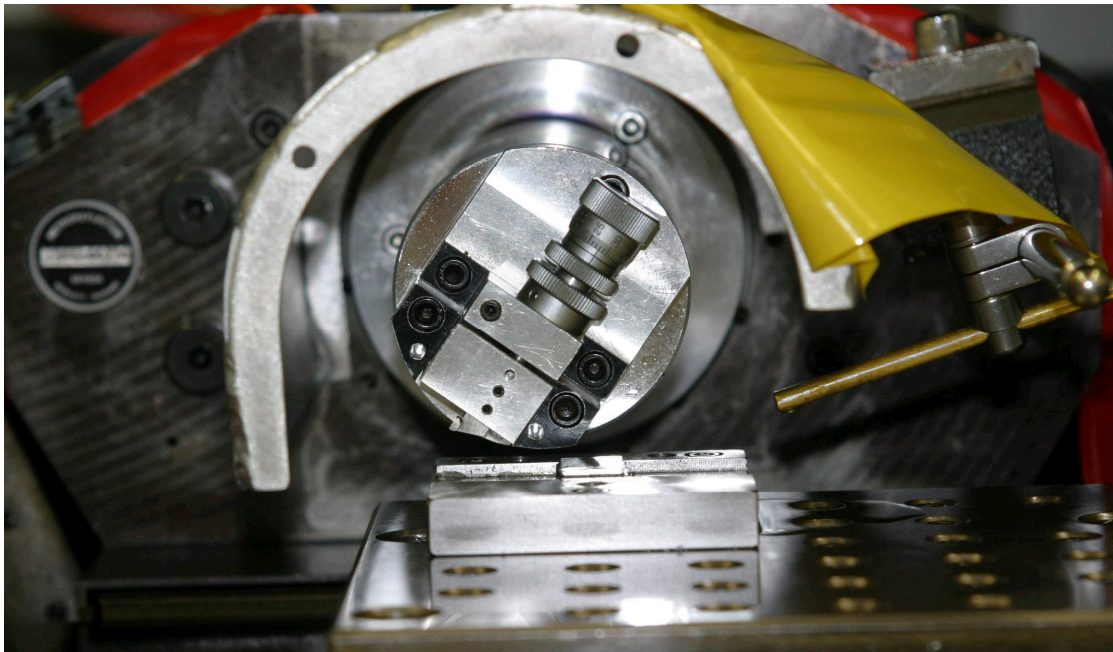
Figure 9. Photo taken during the machining process shows the tip of the diamond tool extending from a holder on the rotating spindle. A spray of light mineral oil from the right acts as a coolant and cutting fluid as well as clearing chips from the workpiece.
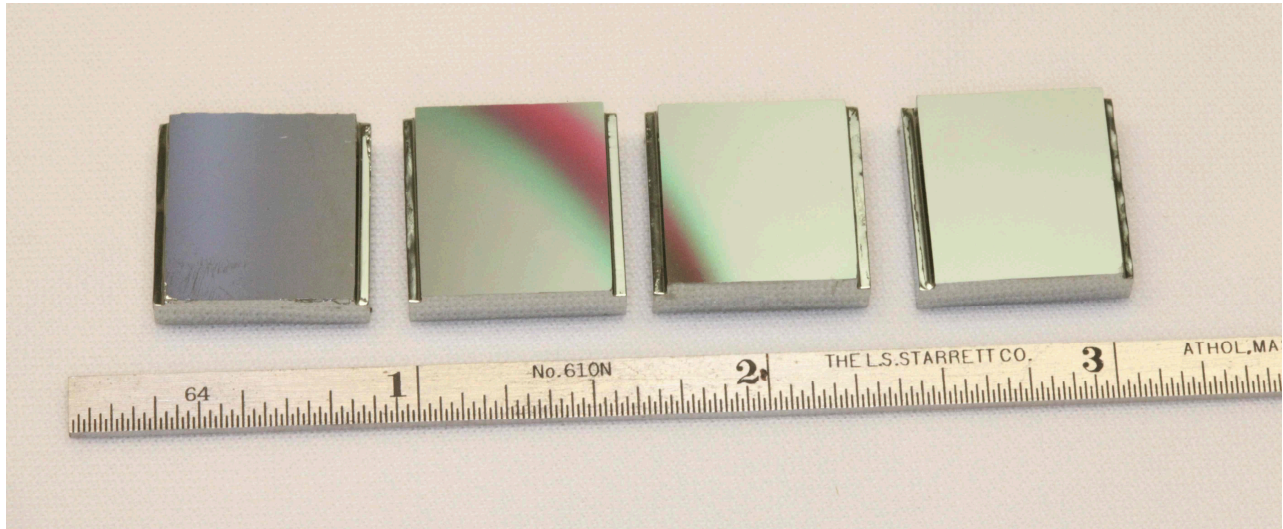
Figure 10. Photograph of 4 of the 6 grisms (#1, 3, 5 and 6). The other two (#2, 4) were installed in LMIRcam for testing.
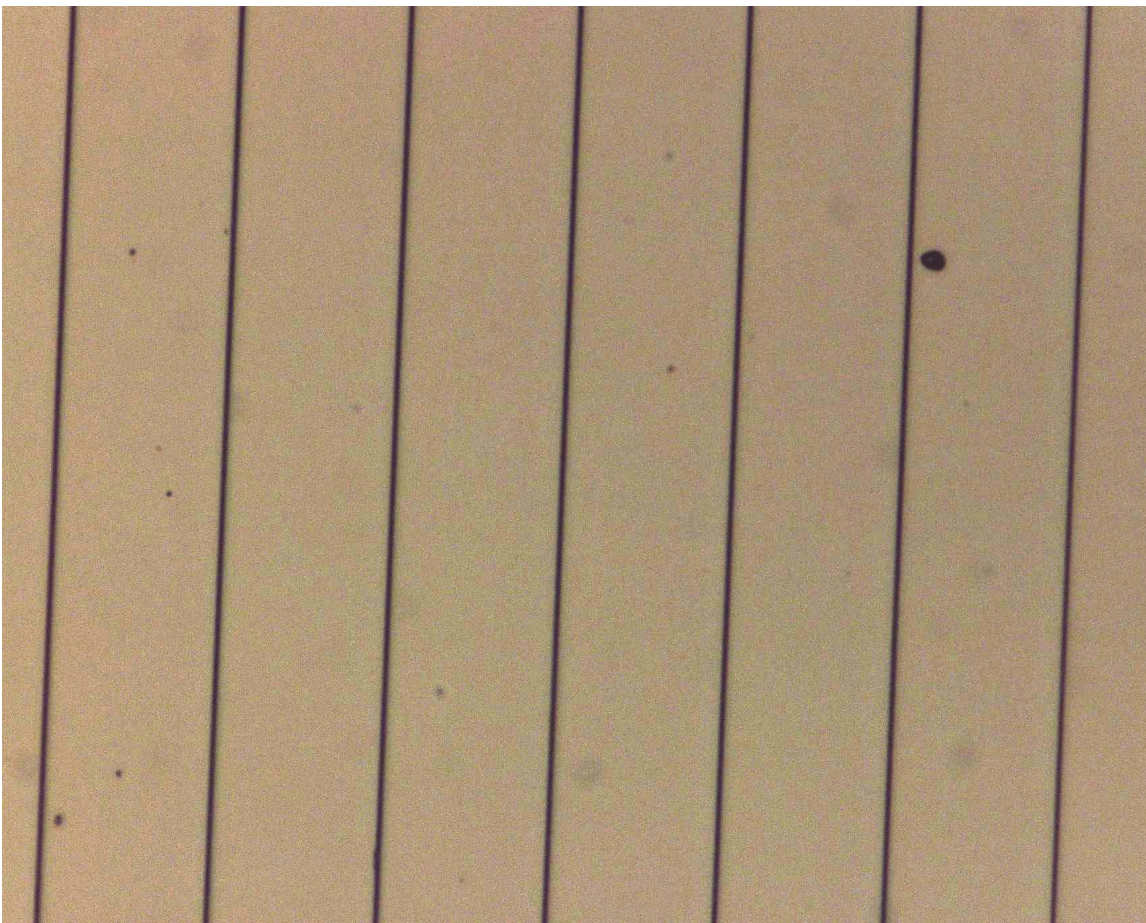

Figure 11. Optical photograph shows the machined surface of grism #1 at 500x magnification. The groove spacing is 25 μm.
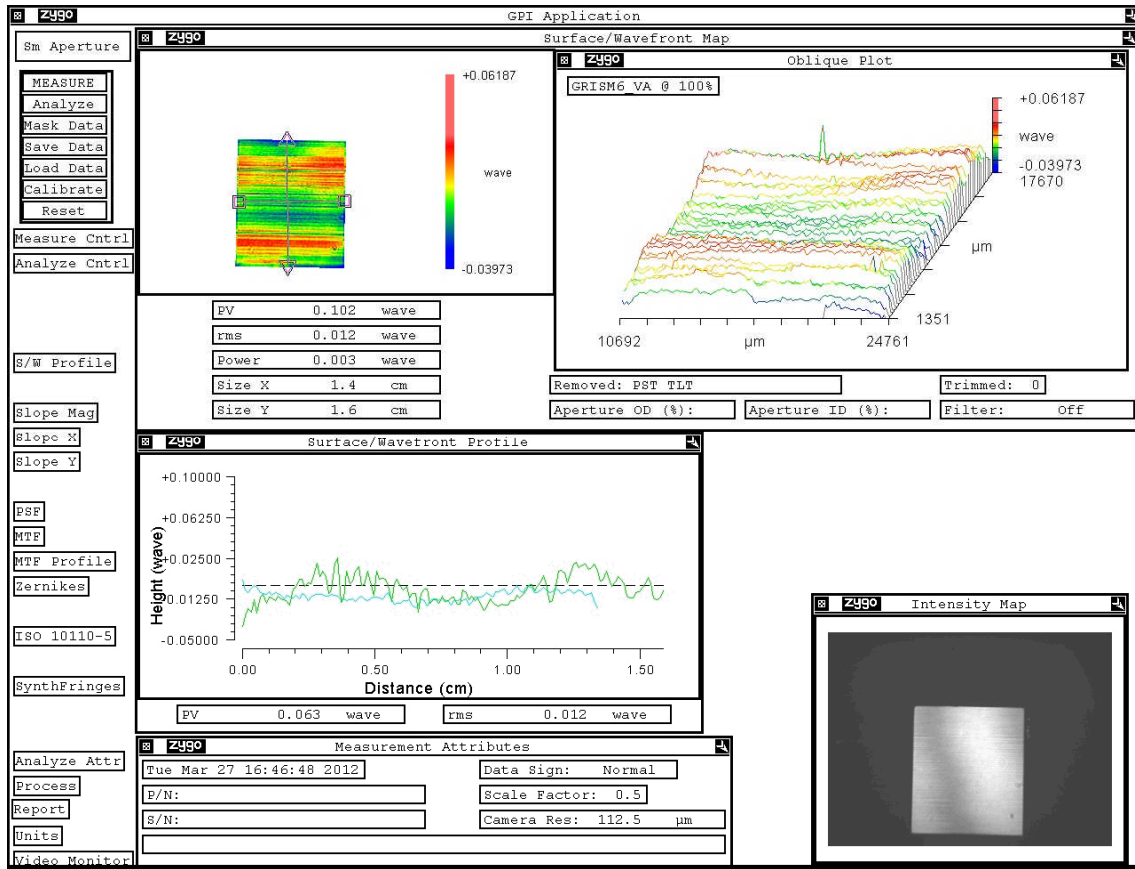
Figure 12. Zygo interferometer measurement on grism #6 shows surface error in grooves to be 0.10λ peak to valley (0.012λ rms) at 633 nm over the full 14 x 14 mm aperture of the grism.
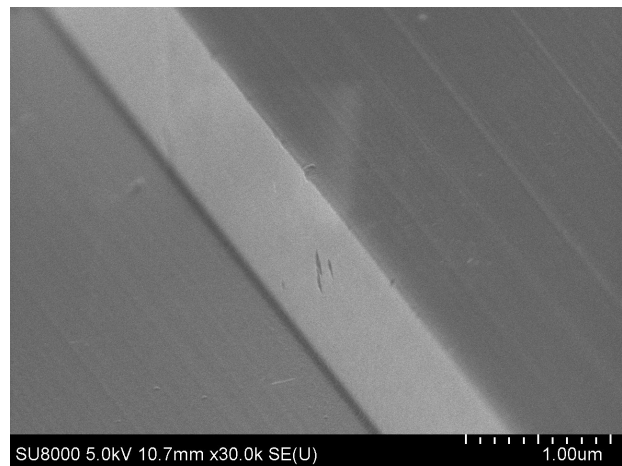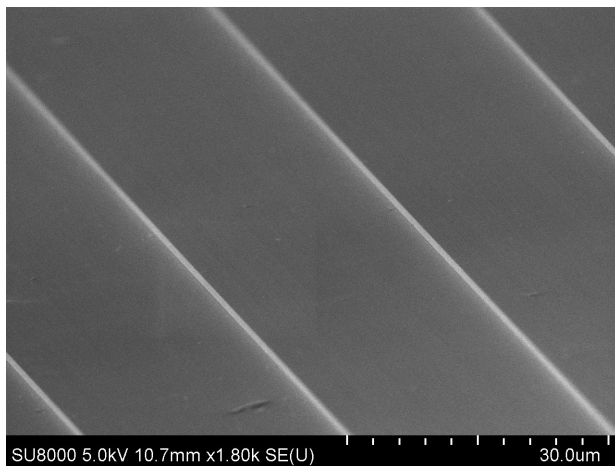
Figures 13 and 14. SEM photos of grism #3 (40 lines/mm). On the left are details of several grooves showing the very flat and smooth blazed surfaces. On the right is a magnified view of a single groove showing the very sharp groove angle.
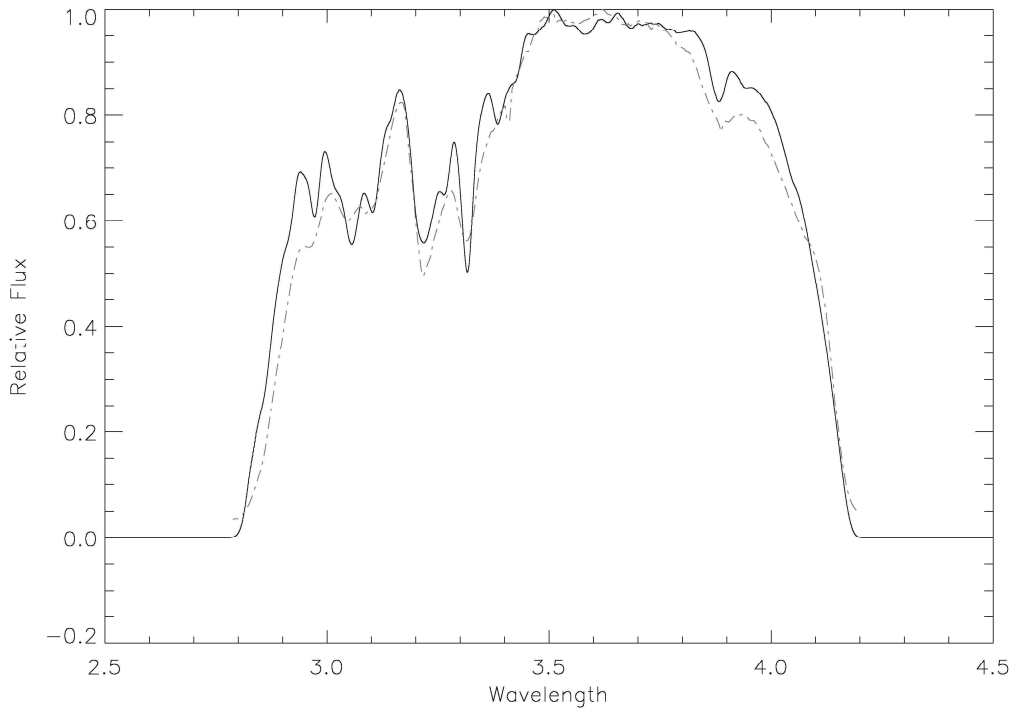
Figure 15: Preliminary extraction of the on-sky, nod-subtracted, observation of the bright star HD 82198 (dash-dot line) taken with LMIRcam L-band grism. Integration time is 29 msec with coherently combined light from both AO-corrected apertures. Overplotted (solid line) is a smoothed ATRAN sky transmission model (courtesy of Gemini Observatory) multiplied by the expected grism efficiency function and transmission functions of a dichroic and order sorting filter in the optical train. The extracted spectrum has been scaled and shifted by eye to approximately match absorption features in the transmission spectrum.
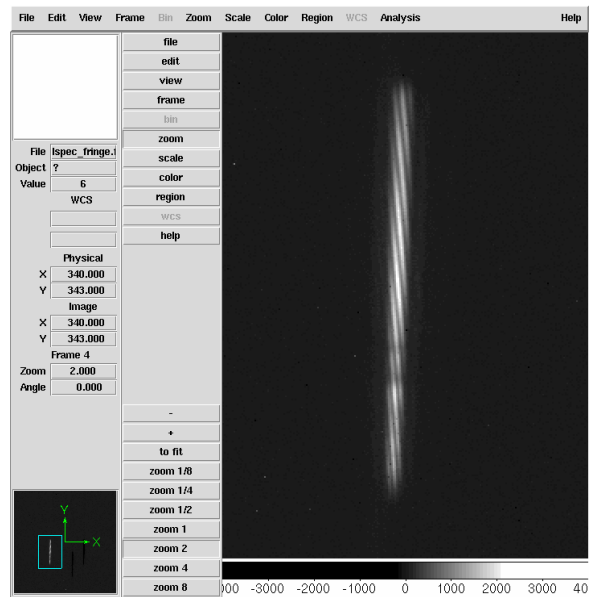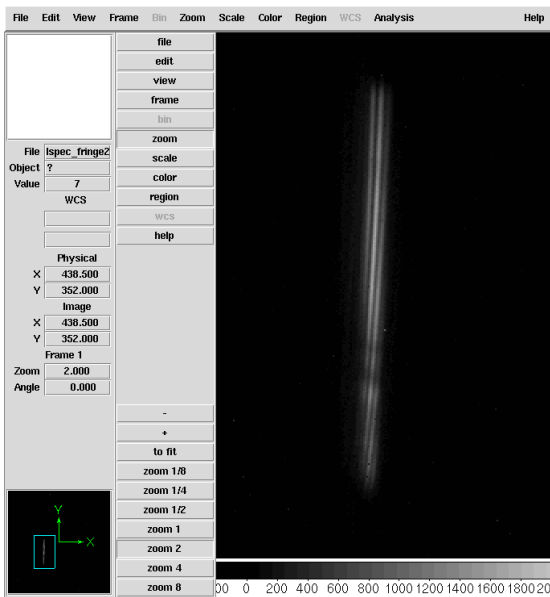
Figures 16 and 17. First results of grism testing in LMIRcam demonstrating the use of the dispersed L-band light to correct the phase delays between apertures. (left) correctly phased and (right) out of phase.